Results in Physics 10 (2018) 99–106

Contents lists available at ScienceDirect

Results in Physics

journal homepage: www.elsevier.com/locate/rinp

Anti-corrosion properties of the symbiotic effect of *Rosmarinus officinalis* and trypsin complex on medium carbon steel

Roland Tolulope Loto*, Cleophas Akintoye Loto

Department of Mechanical Engineering, Covenant University, Ota, Ogun State, Nigeria

ARTICLE INFO

Keywords:
Corrosion
Carbon steel
Inhibition
Adsorption

ABSTRACT

The synergistic reaction of *Rosmarinus officinalis* and trypsin complex on the susceptibility of medium carbon steel to interfacial deterioration in 2 M H_2SO_4 and HCl solution was studied using potentiodynamic polarization method, weight loss evaluation, open circuit potential analysis, optical microscopy and ATR-FTIR spectroscopy. Experimental outcome confirmed the effective performance of the admixture with highest inhibition values of 79.72% and 80.85% in H_2SO_4 with anodic type inhibition, 78.88% and 94.17% in HCl with cathodic type inhibition from the electrochemical tests. The inhibiting compound significantly influenced the thermodynamic behaviour of the steel, shifting the corrosion potential of the steels due to its passivation characteristics. Chemisorption adsorption mechanism was observed with respect to Langmuir and Frumkin adsorption isotherms, and correlation coefficients of 0.8359 and 0.9559 in H_2SO_4 solution, and 0.9900 and 0.9991 in HCl solution respectively. Identified functional groups from ATR-FTIR spectroscopic analysis partially adsorbed onto the carbon steel in H_2SO_4 and completely in HCl. Micro-analytical images of the admixture protected steel contrast the uninhibited.

Introduction

Carbon steels are extensively applied metallic alloy for structural applications and industrial processes due to its relatively low price, ready occurrence and easy formability [1]. The dominant problem encountered during utilization is their low corrosion resistance in aqueous environments. Aqueous acid solutions are extensively employed in industrial operations e.g. industrial inorganic deposit removal, pickling, descaling, and drilling operations during oil and gas inspections, as such carbon steels within these environments are subject to corrosion [2]. Corrosion of carbon steels have received huge attention world-wide due to their economic and safety consequences resulting from rapid damage. Corrosion inhibitors have been proven over the years to be the most cost effective method of corrosion control of carbon steels, however the use of some of the widely available inhibitor formulations commercially have adverse and unsustainable environmental impact. Inorganic chemical inhibitors containing phosphate, chromate, and other heavy metals tops the list of toxic chemicals to the environment, carcinogenic effect and difficulties encountered in their disposal [3,4]. Organic inhibitors have also been extensively used but their application is limited due to their toxicity and high manufacturing cost [5–8]. In view of this naturally occurring biodegradable products lacking heavy metals constituents and toxic compounds is the most promising alternative, among which plant extracts find a prominent place. Previous research has shown that the available phytochemical constituents of plant extracts are inexpensive, non-toxic and readily available source of green chemicals for corrosion inhibition [9,10]. Previous research separately studied the corrosion inhibition properties of *Rosmarinus officinalis* and *Ricinus communis* in weak aqueous solutions with good results [11,12]. This investigation is designed to assess the synergistic corrosion inhibition properties of *Rosmarinus officinalis* and trypsin complex in 2 M H_2SO_4 and HCl solution.

Experimental methods

Materials and preparation

Medium carbon steel (MCS) of cylindrical shape sourced commercially has a nominal composition (wt%) consisting of 0.3% C, 0.6% Mn, 0.15% Ni, 0.04% P, 2.2% Si, 0.5% Cu, 0.03% Mo and 96.18% Fe. The steel specimens with mean dimension of 0.71 cm (thickness), 1.4 cm (diameter) and 5.94 cm^2 (surface area) were grinded after sectioning with silicon carbide abrasives having grit sizes of 80, 120, 220, 320, 600, 800 and 1000. They were afterwards cleansed with deionized water and ketone propane for weight loss analysis and potentiodynamic polarization as stated in ASTM G1-03 (2011) [13]. *Rosmarinus officinalis*

* Corresponding author.
E-mail address: tolu.loto@gmail.com (R.T. Loto).

https://doi.org/10.1016/j.rinp.2018.05.028
Received 9 April 2018; Accepted 16 May 2018
Available online 23 May 2018

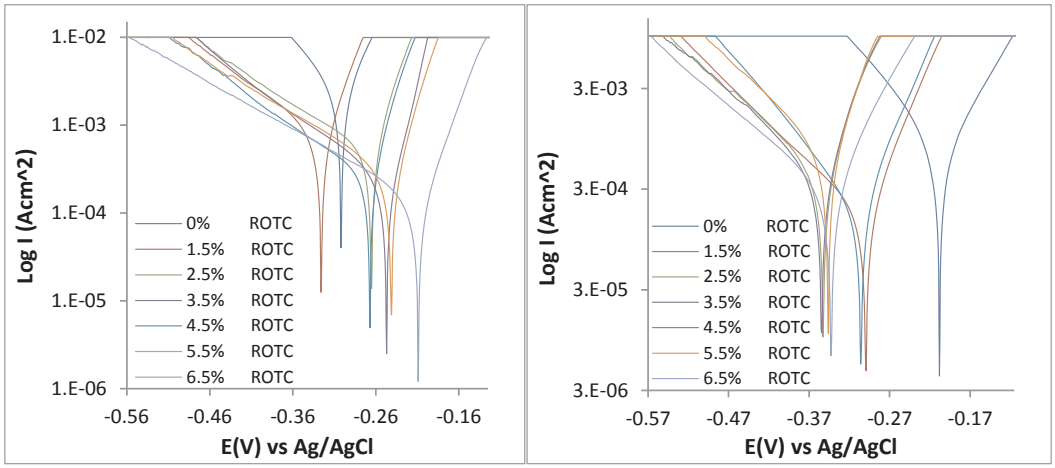

(a) (b)

Fig. 1. Graphical plot of the anodic-cathodic polarization curves for MCS at 0%–6.5% ROTC (a) 2 M H_2SO_4, (b) 2 M HCl solutions.

and trypsin complex obtained from NOW Foods, USA and Bell Sons and Co. UK are the organic compounds evaluated for their inhibition performance. *Rosmarinus officinalis* has a molar mass of has a molar mass (active groups) of 691.14 g/mol, while trypsin complex has a molar mass of 933.45 g/mol. Their combined admixture (ROTC) in similar quantities (1:1) was prepared in molar concentrations of 9.23×10^{-3}, 7.69×10^{-3}, 1.08×10^{-2}, 1.38×10^{-2}, 1.69×10^{-2} and 2.00×10^{-2} in 200 mL of 2 M H_2SO_4 and HCl solution (analar grade) with distilled water.

Potentiodynamic polarization test

Polarization measurement was conducted at 30 °C ambient temperature with the aid of platinum counter electrode, Ag/AgCl reference electrode containing 3 M KCl solution at 6.5 pH and resin embedded circular MCS working electrodes (surface area of 1.54 cm^2) inside a transparent container with 200 mL of H_2SO_4/ROTC and HCl/ROTC test media and linked to Digi-Ivy 2311 potentiostat. Graphical plots of anodic-cathodic polarization diagrams were produced at 0.0015 V/s scan rate at potentials between −1.2 V and 0.5 V [14,15]. Corrosion current density J_c, (A/cm^2) and corrosion potential, E_c (V) were evaluated by Tafel extrapolation. Corrosion current, I_c (A) was determined from the cut of between the cathodic and anodic polarization curves [16,17]. Corrosion rate values, C_{RT} (mm/y) were calculated from the following equation;

$$C_{RT} = \frac{0.00327 \times J_c \times E_q}{D} \quad (1)$$

where E_q is the equivalent weight of MCS (g), 0.00327 is a corrosion rate constant [18], and D is the density (g/cm^3) Inhibition efficiency, IN_{EF} (%) was computed from corrosion rate (Eq. (2));

$$IN_{EF} = \left[1 - \left(\frac{C_{R2}}{C_{R1}}\right)\right] \times 100 \quad (2)$$

C_{R1} is the weight loss without ROTC and C_{R2} is the weight loss with ROTC. Polarization resistance, R_p, (Ω) was computed from Eq. (3);

$$R_p = 2.303 \frac{B_a B_c}{B_a + B_c}\left(\frac{1}{I_{cr}}\right) \quad (3)$$

where B_a is the anodic Tafel slope (V/dec) and B_c is the cathodic Tafel slope (V/dec).

Weight loss analysis

MCS specimens hanged and submerged inside 200 mL of 2 M H_2SO_4 and HCl solution for 240 h were measured every 24 h [19]. Corrosion rate, C_{RT} (mm/y) was determined from the equation below [20],

$$C_R = \left[\frac{87.6 W_L}{DAt}\right] \quad (4)$$

W_L is the weight loss (g), D is the density (g/cm^3), A is the total exposed surface area of MCS sample (cm^2) and 87.6 is a constant. t is the time (h). Inhibition efficiency (IN_{EF}) was computed from the formula below;

$$IN_{EF} = \left[\frac{W_{L1} - W_{L2}}{W_{L1}}\right] \times 100 \quad (5)$$

W_{L1} and W_{L2} are the weight loss at specific ROTC concentrations. Surface coverage was computed from Eq. (6) [21,22]:

$$\theta = \left[1 - \frac{\omega_2}{\omega_1}\right] \quad (6)$$

where θ is the degree of ROTC coverage on MCS. W_{L1} and W_{L2} are the weight loss of each MCS at predetermined ROTC concentration in 2 M H_2SO_4 and HCl solution.

ATF-FTIR spectroscopic studies and optical microscopy analysis

2 M H_2SO_4 and HCl solutions with ROTC compound at specific values, prior to and corrosion test were analysd with Bruker Alpha FTIR spectrometer at 375 to 7500 cm^{-1} wavelength and 0.9 cm^{-1} resolution. The ATF-FTIR absorption graphs of spectra peaks were evaluated and matched with the ideal ATF-FTIR for active molecular group identification involved in the corrosion inhibition of MCS. Micro-analytical images of corroded MCS surface features and ROTC protected MCS were studied after corrosion using Omax trinocular metallurgical microscope.

Results and discussion

Potentiodynamic polarization studies

Potentiodynamic polarization curves of MCS in 1 M H_2SO_4 and HCl solution at 0%–6.5% ROTC concentration are shown in Fig. 1(a) and (b). Data obtained from the polarization test are depicted in Table 1. MCS corroded at a much higher rate in H_2SO_4 (20.19 mm/y) compared to HCl solution (11.01 mm/y) at 0% ROTC due to the higher ionization strength of H_2SO_4 in H_2O releasing two protons which strongly reacts and deteriorates MCS surface compared to HCl which gives out one proton. Comparison of the corrosion potential at this concentration shows MCS tends to be significantly electronegative in H_2SO_4 than in

Table 1
Potentiodynamic polarization data for MCS in 2 M H_2SO_4 and HCl solution in 0%–6.5% ROTC concentration.

Sample	ROTC Conc. (%)	ROTC Conc. (M)	C_{RT} (mm/y)	IN_{EF} (%)	I_c (A)	J_c (A/cm^2)	E_c (V)	R_p (Ω)	B_c (V/dec)	B_a (V/dec)
2 M H_2SO_4 solution										
A	0	0	20.19	0	2.68E−03	1.74E−03	−0.302	10.19	−7.616	12.044
B	2	9.23E−03	10.00	50.45	1.33E−03	8.62E−04	−0.326	51.56	−6.226	7.875
C	3	7.69E−03	5.43	73.12	7.20E−04	4.68E−04	−0.265	91.22	−5.583	6.941
D	4	1.08E−02	4.95	75.51	6.57E−04	4.26E−04	−0.247	104.45	−5.075	6.118
E	5	1.38E−02	4.64	77.00	6.16E−04	4.00E−04	−0.267	110.61	−5.138	6.217
F	6	1.69E−02	4.09	79.72	5.44E−04	3.53E−04	−0.241	122.82	−5.347	6.556
G	7	2.00E−02	4.21	79.16	5.59E−04	3.63E−04	−0.209	115.65	−5.183	6.358
2 M HCl solution										
A	0	0	11.01	0	1.46E−03	9.49E−04	−0.208	195.91	−6.205	5.910
B	2	9.23E−03	3.11	71.80	4.12E−04	2.68E−04	−0.299	38.27	−7.413	3.560
C	3	7.69E−03	2.93	73.35	3.90E−04	2.53E−04	−0.353	34.87	−7.903	3.377
D	4	1.08E−02	2.98	72.91	3.96E−04	2.57E−04	−0.354	29.35	−8.302	3.138
E	5	1.38E−02	2.77	74.83	3.68E−04	2.39E−04	−0.306	28.73	−10.460	3.190
F	6	1.69E−02	2.33	78.88	3.09E−04	2.00E−04	−0.346	38.55	−7.860	3.118
G	7	2.00E−02	2.32	78.93	3.08E−04	2.00E−04	−0.343	43.91	−6.797	3.150

HCl for reasons earlier mentioned, which corresponds to a higher corrosion current density and significantly higher anodic Tafel slope value. The anodic exchange current density is greater than the cathodic counterpart in H_2SO_4 but lower in HCl due to the predominant oxidation reaction in H_2SO_4.

Addition of ROTC compound to the acid solutions (H_2SO_4 and HCl) changed the mechanism of the redox electrochemical interaction. In H_2SO_4 corrosion suppression by ROTC compound at 1.5% concentration is marginal and the corrosion potential shifts to a cathodic value of −0.326 V from −0.302 V at 0% ROTC. There is a remarkable change in anodic Tafel slope from 12.044 V/dec to 7.875 V/dec (1.5% ROTC) signifying anodic inhibition due to surface coverage. Further increase in ROTC concentration in H_2SO_4 solution results in average inhibition efficiency above 70% till 6.5% ROTC concentration. The anodic and cathodic Tafel slopes beyond 1.5% ROTC remained slightly the same, corresponding to near similar values of ROTC inhibition efficiency. This confirms the earlier mention assumption of corrosion inhibition by interfacial covering whereby the molecular movement of corrosive species unto MCS solution interface is limited. Changes in corrosion potential beyond 1.5% ROTC further confirms the inhibition mechanism of ROTC in H_2SO_4 as the corrosion potential transits to anodic values due to inhibition of anodic dissolution reactions.

Observation of the corrosion potential values of MCS in HCl shows a significant shift to cathodic potentials from −0.208 V at 0% ROTC to −0.343 V at 6.5% ROTC, signifying dominant cathodic inhibition properties of ROTC in HCl. Changes in cathodic Tafel slope values with respect to ROTC concentration confirms this assumption. Despite the relatively lower corrosion rate value in HCl solution at 0% ROTC, the inhibition efficiency values of ROTC are comparable to the values obtained in H_2SO_4 due to the relatively lower inhibition performance of ROTC in the solution simply because ROTC protonates more strongly in H_2SO_4 causing excess of electrons from molecules. This paradox causes the compound to be more reactive resulting in strong interaction with MCS surface. The peak anodic shift in corrosion potential of MCS in H_2SO_4 is 93 mV and 146 mV cathodicaly in HCl, thus ROTC is an anodic type inhibitor in H_2SO_4 and a cathodic type inhibitor in HCl [23].

Weight-loss analysis and Micro analytical studies

Results obtained for MCS weight-loss (W_L), corrosion rate (C_R) and ROTC inhibition efficiency (IN_{EF}) in 2 M H_2SO_4 and HCl solution at 240 h exposure time is shown in Table 2. Fig. 2(a) to 3(b) present the graphical curves of MCS corrosion rate and ROTC inhibition efficiency against exposure time in 2 M H_2SO_4 and HCl solution. Optical representations and morphological characteristics of MCS prior to corrosion, after corrosion, in the presence and absence of ROTC inhibitor

Table 2
Experimental results from weight loss measurement at 240 h for MCS corrosion in 2 M H_2SO_4 and HCl solution at 0%–6.5% ROTC).

MCS Samples	Weight Loss (g)	ROTC Concentration (%)	ROTC Concentration (M)	C_{RT} (mm/yr)	ROTC IN_{EF} (%)
2 M H_2SO_4					
A	3.788	0	0	29.650	0
B	1.812	1.5	9.23E−03	14.186	52.15
C	0.847	2.5	7.69E−03	6.626	77.65
D	0.841	3.5	1.08E−02	6.582	77.80
E	0.760	4.5	1.38E−02	5.950	79.93
F	0.725	5.5	1.69E−02	5.677	80.85
G	0.974	6.5	2.00E−02	7.624	74.29
2 M HCl					
A	2.957	0	0	23.144	0
B	0.487	1.5	9.23E−03	3.812	83.53
C	0.410	2.5	7.69E−03	3.205	86.15
D	0.358	3.5	1.08E−02	2.802	87.89
E	0.172	4.5	1.38E−02	1.349	94.17
F	0.319	5.5	1.69E−02	2.494	89.22
G	0.378	6.5	2.00E−02	2.955	87.23

from both acids are depicted from Fig. 4(a) to 5(d) at ×40 magnification. MCS corrosion rate value in H_2SO_4 at 0% ROTC concentration showed corrosion behaviour of the steel was unstable [Fig. 2(a)] for the first 72 h, shifting from 0.0320 mm/y through 0.0374 mm/y to 0.0320 mm/y. A gradual decline in corrosion rate was later observed till 168 h at 0.0293 mm/y before mild variation in corrosion rate values till 240 h. This observation significantly contrasts the plots obtained for MCS in HCl solution [Fig. 2(b)] where the corrosion rate sharply increased after 24 h of exposure due to the electrochemical action of Cl^- anions on MCS corrosion which tends to be more debilitating than SO_4^{2-} anions. The corresponding optical morphology of MCS after corrosion in both acids (0% ROTC) is shown in Fig. 4(b) and 5(b), which significantly contrast the morphology before corrosion [Fig. 4(a) and 5(a)]. Though the morphology of Fig. 4(b) and 5(b) are severely corroded, Fig. 5(b) shows the presence of corrosion pits due to the relatively small size of Cl^- anions (in comparison to SO_4^{2-} anions) which enables penetration through the metal substrate. This is responsible for the consistent increase in corrosion rate of MCS in HCl solution. Addition of ROTC to the acid solutions changed the reaction mechanism within the solutions. In H_2SO_4 solution ROTC acted instantaneously, achieving relative stability in inhibiting the corrosion and anodic dissolution of MCS after 48 h of exposure when compared to its action in HCl and its inhibition efficiency tends to be negligibly proportional to its concentration after 1.5% ROTC. The optical microscopy morphology

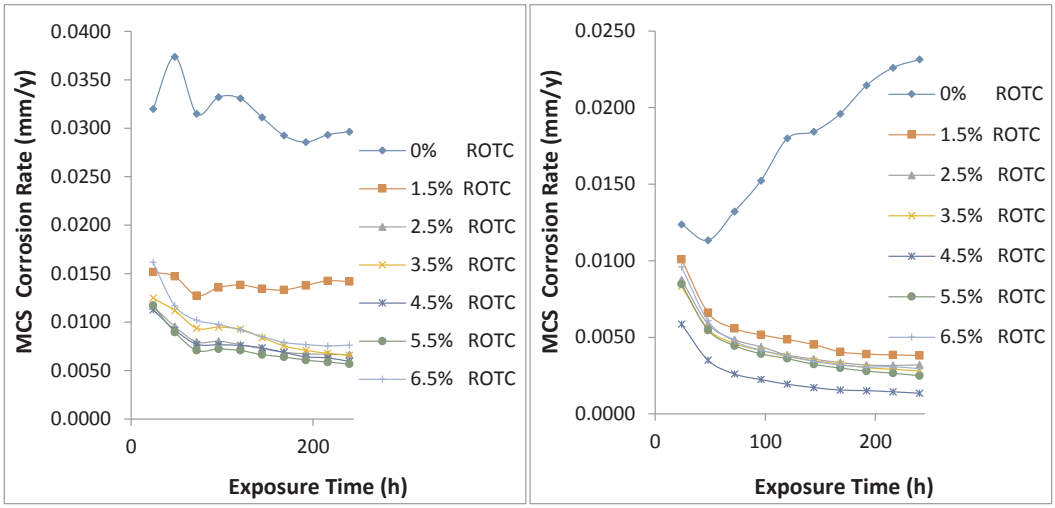

(a) (b)

Fig. 2. Graphical curves of (a) MCS corrosion rate against exposure time in (a) 2 M H_2SO_4 (b) 2 M HCl.

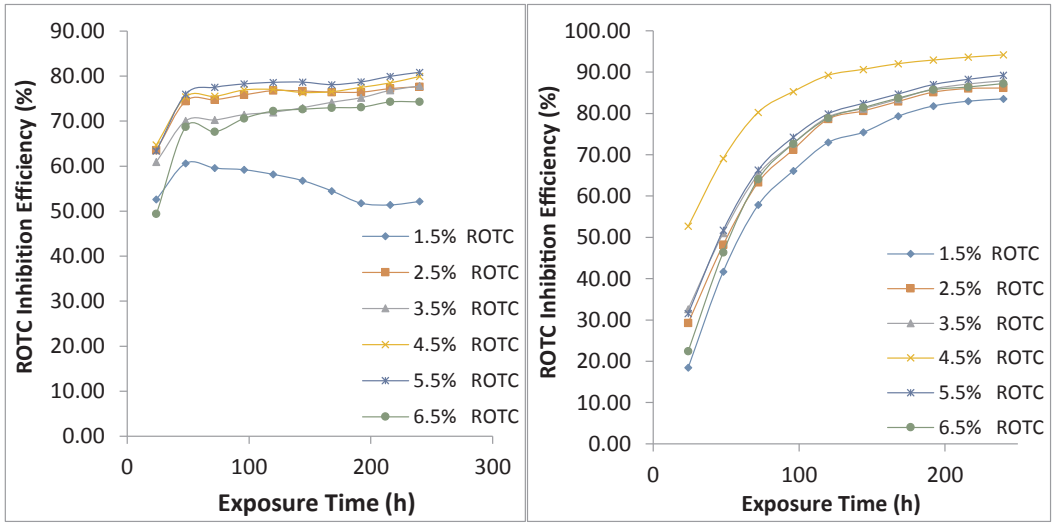

(a) (b)

Fig. 3. Graphical curves of (a) ROTC inhibition efficiency against exposure time in (a) 2 M H_2SO_4 (b) 2 M HCl.

in Fig. 4(c) and (d) shows a mildly deteriorated surface at 1.5% and 6.5% ROTC, possibly as a result of pre-adsorbed anions of sulphate prior to adsorption of ROTC molecules. This suppressed the redox electrochemical reactions responsible for corrosion. In HCl there is a consistent increase in ROTC inhibition efficiency with respect to exposure time till 240 h and the inhibition efficiency values is appreciably higher than values obtained in H_2SO_4. The optical microscopy morphology in Fig. 5(c) and (d) shares similar characteristics with the images obtained in H_2SO_4.

Open circuit potential measurement

The thermodynamic tendency of MCS to corrode with respect to it aqueous environment is shown on the graphical plots of corrosion potential versus exposure time for MCS in 2 M H_2SO_4 and HCl solution at 0%, 1.5% and 6.5% ROTC for 1800 s [Fig. 6(a) and (b)]. The corrosion potential values for MCS in 2 M H_2SO_4/ 0% ROTC proves to be less thermodynamically stable than the values obtained at 2 M H_2SO_4/ 1.5% and 6.5% ROTC due to visible potential transients. Its corrosion potential initiated at $-0.268V_{Ag/AgCl}$ at 0 s and stopped at $-0.265V_{Ag/AgCl}$ at 1800 s. The observed potential transients are as a result of the currents flowing from localized corrosion sites on MCS. Addition of ROTC compound at 1.5% and 6.5% shifted the corrosion potential of MCS to $-0.231V_{Ag/AgCl}$ and $-0.213V_{Ag/AgCl}$, making the steel more thermodynamically stable and reducing its tendency to corrosion as a result of changes in the reactions of SO_4^{2-} induced redox processes. The shift in open circuit potential plots of MCS at 1.5% and 6.5% ROTC shows anodic inhibition by ROTC compound confirming earlier results from potentiodynamic polarization. The corrosion potential plot of 6.5% ROTC shows its equilibrium state is unstable despite increased passivation of MCS due to corrosion inhibition. The open circuit potential plots of MCS in 2 M HCl solution significantly contrast the plots in 2 M H_2SO_4 solution. At 0% ROTC, the corrosion potential starts at $-0.310V_{Ag/AgCl}$ (0 s) and shifts anodically till $-0.304V_{Ag/AgCl}$ at 1800 s. The visible current transients are due to the electrochemical action of Cl^- anions on MCS surface which in effect makes the steel thermodynamically unstable, increases its tendency to corrode and clearly signifies that the steel is not in equilibrium within the HCl solution. Similar active passive behaviour was observed for MCS at 1.5% and 6.5% ROTC concentration, however the presence of ROTC shifts the

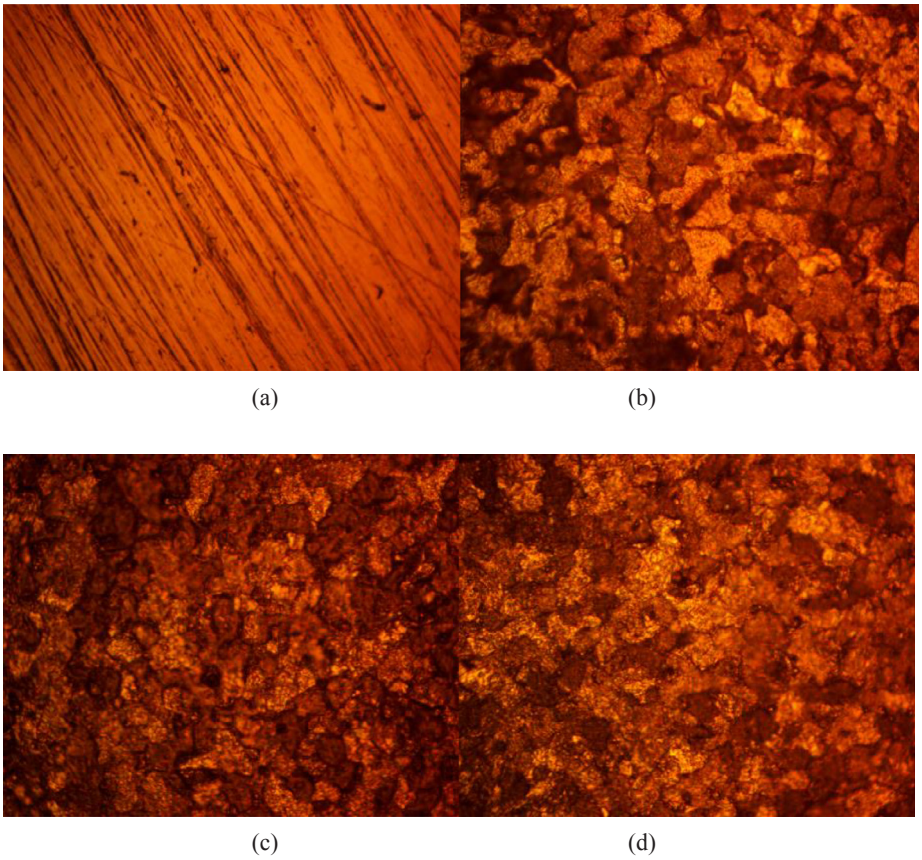

Fig. 4. Morphology of MCS at mag. ×40 from 2 M H_2SO_4 solution (a) before corrosion, (b) after corrosion at 0% ROTC, (c) after corrosion at 1.5% ROTC and (d) after corrosion at 6.5% ROTC.

corrosion potential cathodically signifying cathodic inhibition as earlier determined from potentiodynamic polarization hence the corrosion behaviour of MCS in the presence of ROTC compound is the same in free and applied potential monitoring.

Adsorption isotherm

The adsorption and corrosion inhibition of ROTC on the electrochemical behaviour of MCS occurred through the reaction mechanism whereby ROTC transferred its proton to the vacant orbitals (due to oxidation reaction) of MCS forming a coordinate bond over the entire MCS surface. This is possible through molecular reactions involving charge transfer. The mechanism of ROTC adsorption was further determined and studied through adsorption isotherms. Studies show ROTC fits well with the Langmuir and Frumkin adsorption isotherm models in both acid solutions with correlation coefficients of 0.8359 and 0.9559 in H_2SO_4 solution, and 0.9900 and 0.9991 in HCl solution respectively. Other isotherms tested (Freundlich and Temkin) gave correlation coefficients below 0.3 which is far from unity.

The Langmuir isotherm plot of $\frac{C_{ROTC}}{\theta}$ versus C_{ROTC} [Fig. 7(a) and (b)], determined from Eq. (7) suggests; (i) Molecular interaction on the metal surface is invariable, (ii) Gibbs free energy is non-dependent on the extent of adsorbates coverage and (iii) Effect of Lateral interaction due to reaction of molecular species is negligible on the value of Gibbs free energy [24]. The Frumkin plot of Log $\frac{\theta}{1-\theta}$ versus Θ [Fig. 8(a) and (b)], determined from Eq. (8) assumes complete molecular coverage when the concentration of ROTC is high for non-homogeneous metal alloys and the lateral interaction effect is negligible.

$$\theta = \left[\frac{K_{ads} C_{ROTC}}{1 + K_{ads} C_{ROTC}}\right] \quad (7)$$

$$\mathrm{Log}[C_{ROTC} * (\theta/1-\theta)] = 2.303 \log K_{ads} + 2\alpha\theta \quad (8)$$

Thermodynamics of the corrosion process

The energy of molecular interaction responsible for ROTC corrosion inhibition and surface adsorption onto MCS is commensurate to the amount of H_2O molecules (n) displaced by ROTC in the acid media. Molecular adsorption of organic compounds is a replacement reaction which involves removal of H_2O molecules from the steel surface and is commensurate to the amount of metallic cations passed into the electrolyte, and degree of ROTC coverage. Calculated data of Gibbs free energy (ΔG^o_{ads}) for the molecular interaction are presented in Table 3 and were calculated from the Eq. (9) [25].

$$\Delta G_{ads} = -2.303RT \log[55.5 K_{ads}] \quad (9)$$

55.5 is a constant for molar concentration of water in the solution, R is the universal gas constant, T is the absolute temperature and K_{ads} is the equilibrium constant of adsorption. K_{ads} is related to surface coverage (θ) from the Langmuir equation (Eq. (7)).

The heterogeneous nature and surface properties of MCS has a strong influence on ΔG^o_{ads} values with respect to the degree of ROTC surface coverage value. The negative values of ΔG^o_{ads} show adsorption mechanism is random and progression of the molecular film layer on the metal surface. The highest ΔG^o_{ads} value obtained for ROTC adsorption on MCS in H_2SO_4 and HCl solution is $-42.22\,\mathrm{KJ\,mol^{-1}}$ at 2.5% ROTC and $-44.57\,\mathrm{KJ\,mol^{-1}}$ at 4.5% ROTC, while the lowest value in both acids are $-38.89\,\mathrm{KJ\,mol^{-1}}$ at 1.5% ROTC and $-41.53\,\mathrm{KJ\,mol^{-1}}$ at 6.5% ROTC. This is consistent with adsorption mechanism associated with covalent interaction and electrostatic attraction [26,27].

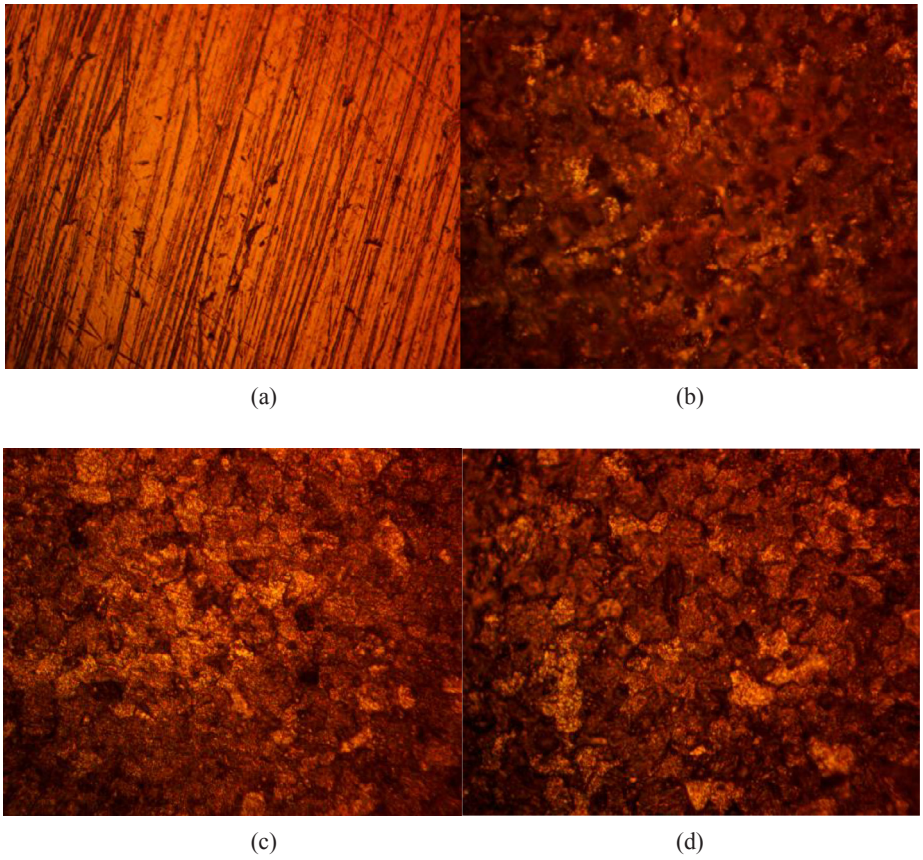

Fig. 5. Morphology of MCS at mag. ×40 from 2 M HCl solution (a) before corrosion, (b) after corrosion at 0% ROTC, (c) after corrosion at 1.5% ROTC and (d) after corrosion at 6.5% ROTC.

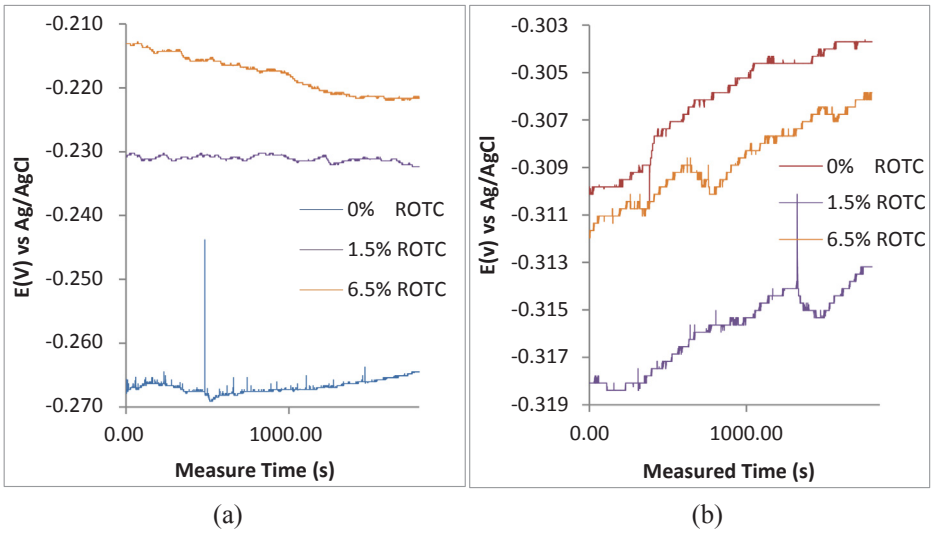

Fig. 6. Fluctuation of corrosion potential vs calibrated time for MCS specimen immersed in (a) 2 M H_2SO_4/0%, 1.5% and 6.5% ROTC, (b) 2 M H_2SO_4/0%, 1.5% and 6.5% ROTC.

ATF-FTIR spectroscopy analysis

Moieties of atoms or bonds within ROTC molecules responsible the adsorption and corrosion inhibition reactions on MCS surface were discovered by ATF-FTIR spectroscopy after comparing with the ATR-FTIR Theoretical Table [28,29]. Fig. 9(a) and (b) shows the graphical curves of the spectrums of 2 M H_2SO_4 and HCl/ROTC solutions before and after MCS corrosion. The transmittance of calculated wavenumbers of 2 M H_2SO_4/ROTC solution before corrosion decreased significantly at wavelengths between of 885.21–2880 cm^{-1} after corrosion as shown on the spectrum of 2 M H_2SO_4/ROTC solution due to adsorption of specific ROTC molecules.

The functional groups identified within the aforementioned wavelength range are alkenes, aldehydes, nitrile, alkynes, esters, saturated aliphatic, carboxylic acids, alpha, beta–unsaturated esters, carbonyls (general), ketones, alpha, beta–unsaturated aldehydes, N—H bend primary amines, aromatics, nitro compounds, alkanes, aromatic amines, alcohols, ethers, alkyl halides, aliphatic amines and secondary amines

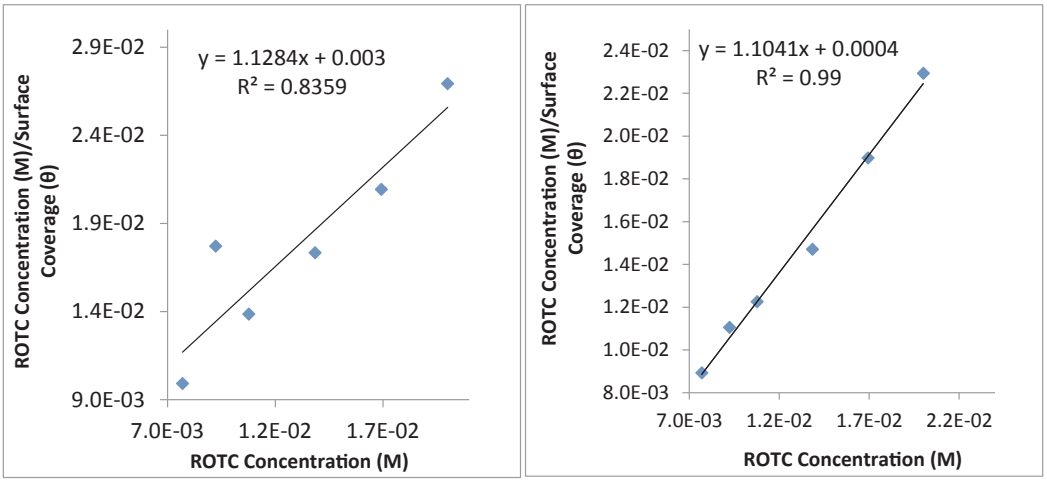

(a) (b)

Fig. 7. Graphical illustration of $\frac{C}{\theta}$ versus ROTC concentration (a) 2 M H_2SO_4 and (b) 2 M HCl.

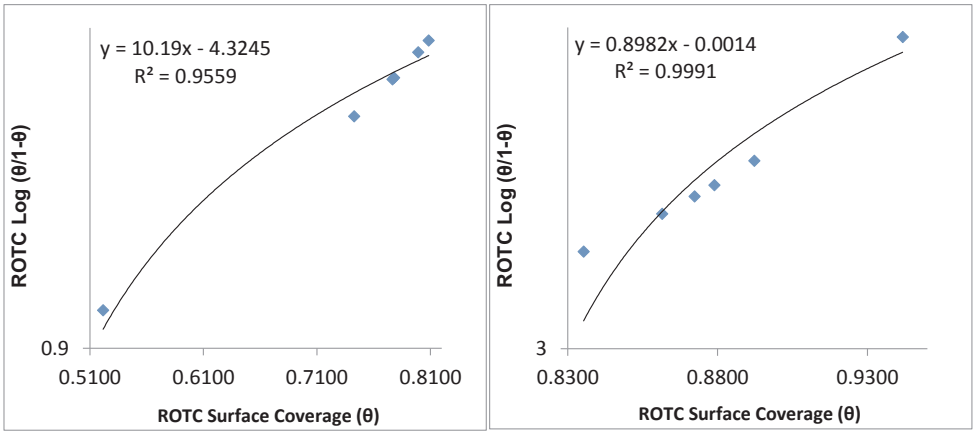

(a) (b)

Fig. 8. Graphical illustration of $\frac{\theta}{1-\theta}$ versus ROTC concentration (a) 2 M H_2SO_4 and (b) 2 M HCl.

Table 3
Result for ΔG^{o}_{ads}, θ and K_{ads} for ROTC adsorption on MCS in 2 M H_2SO_4 and HCl solution.

MCS Samples	ROTC Concentration (M)	θ	K_{ads}	ΔG_{ads} (Kjmol^{-1})
2 M H_2SO_4				
A	0	0	0	0
B	0.0092	0.522	118059.1	−38.89
C	0.0077	0.777	451591.9	−42.22
D	0.0108	0.778	325332.0	−41.41
E	0.0139	0.799	287609.6	−41.10
F	0.0169	0.809	249484.5	−40.75
G	0.0200	0.743	144409.1	−39.39
2 M HCl				
A	0	0	0	0
B	0.0092	0.835	549247.1	−42.70
C	0.0077	0.862	808430.9	−43.66
D	0.0108	0.879	673874.2	−43.21
E	0.0139	0.942	1166830.0	−44.57
F	0.0169	0.892	489166.3	−42.42
G	0.020005	0.872324	341529.7	−41.5256

consisting of bonds such as =C−H stretch, H−C=O: C−H stretch, C(triple bond)N stretch, −C(triple bond)C− stretch, C=O stretch, C=O stretch, −C=C− stretch, C−C stretch (in–ring), N−O asymmetric stretch, C−H bend, C−H rock, N−O symmetric stretch, C−N stretch, C−O stretch, C−H wag (−CH2X), =C−H bend, O−H bend, N−H wag and C−H "oop". Decrease in transmittance of wavenumbers confirmed the effect of surface coverage resulting on MCS surface.

The transmittance of calculated wavenumbers of 2 M HCl/ROTC solution before corrosion decreased at wavelength 520–3638 cm^{-1}, i.e. at a much wider range than in H_2SO_4 solution, thus having similar functional groups involved in corrosion inhibition of MCS in H_2SO_4 in addition to alkyl halides group which consist of C−Cl stretch, C−H rock, −C(triple bond)C−H: C−H bend, C−Br stretch, =C−H stretch, −C(triple bond)C−H: C−H stretch, N−H stretch, O−H stretch, H–bonded and free hydroxyl bonds. This explains the higher surface coverage and corrosion inhibition of ROTC on MCS in HCl solution due to the active participation of additional functional groups in the acid solution.

Conclusion

Corrosion suppression by the combined admixture of *Rosmarinus officinalis* and trypsin complex on medium carbon steel in 2 M H_2SO_4

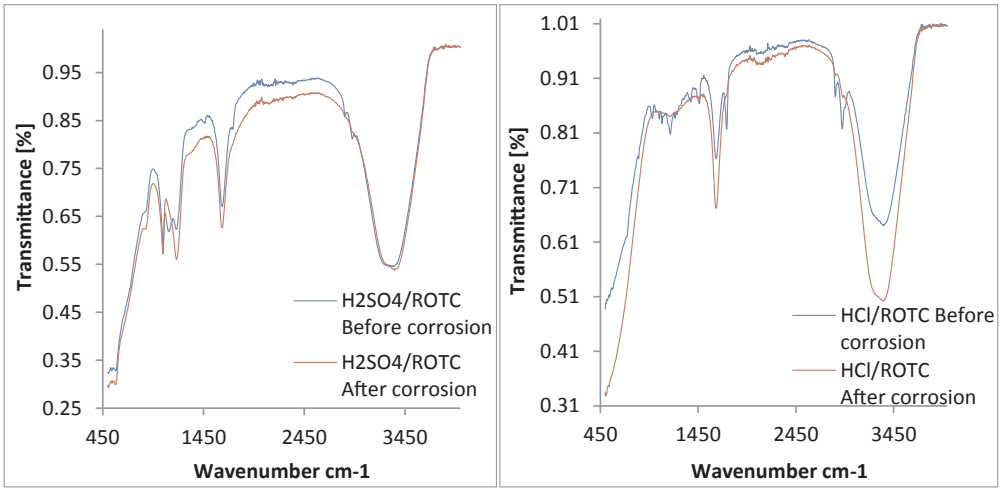

Fig. 9. ATF-FTIR spectra of ROTC on MCS in (a) 2 M H_2SO_4 solution and (b) 2 M HCl solution.

and HCl solution occurred through surface coverage and chemisorption molecular interaction according to the Langmuir and Frumkin isotherm model from potentiodynamic polarization and weight loss and the inhibition type in both acids contrast each other due to different anionic reactions. The chemical compound performed relatively more effectively in HCl solution compared to H_2SO_4 despite the small size of Cl^- compared to SO_4^{2-}. Identified functional groups in the inhibitor adsorbed onto the carbon steel from analysis of the spectrum plots. Optical representations of the protected steel showed moderate morphological deterioration with lean and shallow pits in comparison to the uninhibited steel plagued with severely corroded and pitted surface.

Acknowledgement

The author recognizes the support given by Covenant University Ota, Ogun State, Nigeria towards the sponsorship, implementation and successful completion of the research.

Appendix A. Supplementary data

Supplementary data associated with this article can be found, in the online version, at http://dx.doi.org/10.1016/j.rinp.2018.05.028.

References

[1] Singh DK, Kumar S, Udayabhanu G, John RP. J Mol Liq 2016;216:738.
[2] Raja PB, Sethuraman MG. Mat Lett 2008;62(1):113.
[3] Legault RA, Walker MS. Corrosion 1964;20(9):282t.
[4] Igual Muñoz A. Corros Sci 2007;49(8):3200.
[5] Ortega-Toledo DM, Gonzalez-Rodriguez JG, Casales M, Neri-Flores MA, Martinez-Villafañe A. Mater Chem Phys 2010;122(2–3):485.
[6] Ortega-Sotelo DM, Gonzalez-Rodriguez JG, Neri-Flores MA, Casales M, Martinez L, Martinez-Villafañe A. J Solid State Electrochem 2011;15(9):1997.
[7] Loto RT. Surf Rev Lett 2017;24:7.
[8] Loto RT. Rev Colomb Quim 2017;46(1):20.
[9] Oguzie EE. Corros Sci 2008;50(11):2993.
[10] Bentrah H, Rahali Y, Chala A. Corros Sci 2014;82:426.
[11] El Ouariachi E, Paolini J, Bouklah M, Elidrissi A, Bouyanzer A, Hammouti B, et al. Acta Metall Sinica 2010;23(1):13.
[12] Saratha R, Kasthuri N, Thilagavathy P. Der Pharma Chem 2009;1(2):249.
[13] ASTM G1-03. Standard Practice for Preparing, Cleaning, and Evaluating Corrosion Test Specimens; 2011. http://www.astm.org/Standards/G1.
[14] ASTM G59-97. Standard Test Method for Conducting Potentiodynamic Polarization Resistance Measurements; 2014. http://www.astm.org/Standards/G31.
[15] ASTM G102-89 e1. Standard Practice for Calculation of Corrosion Rates and Related Information from Electrochemical Measurements; 2015. http://www.astm.org/Standards/G31.
[16] Basics of corrosion measurements. http://www.che.sc.edu/faculty/popov/drbnp/ECHE789b/Corrosion%20Measurements.pdf.
[17] Corrosion, Part 2 – Measurement of corrosion rates. http://www.ecochemie.nl/download/Applicationnotes/Autolab_Application_Note_COR02.pdf.
[18] Choi Y, Nesic S, Ling S. Electrochim Acta 2011;56(4):1752.
[19] ASTM G31-72. Standard Practice for Laboratory Immersion Corrosion Testing of Metals; 2004. https://www.astm.org/DATABASE.CART/HISTORICAL/G31-72R04.htm.
[20] Venkatesan P, Anand B, Matheswaran P. Eur J Chem 2009;6(S1):S438.
[21] Schutt HU, Horvath RJ. Crude column overhead corrosion problem caused by oxidized sulfur species. Houston, Texas: NACE; 1987.
[22] Schofield MJ. Plant engineer's reference book. Elsevier; 2003.
[23] Loto RT, Loto CA, Popoola AP. South Afr J Chem 2015;68:105.
[24] Ashish KS, Quraishi MA. Corros Sci 2011;53(4):1288.
[25] Soror TY. J Mater Sci Tech 2004;20(4):463.
[26] Bouklah M, Hammouti B, Lagrene M, Bentiss F. Corros Sci 2006;48(9):2831. http://dx.doi.org/10.1016/j.corsci.2005.08.019.
[27] Loto RT. Cogent Eng 2016;3. http://dx.doi.org/10.1080/23311916.2016.1242107.
[28] Table of Characteristic IR Absorptions. http://orgchem.colorado.edu/Spectroscopy/specttutor/irchart.pdf.
[29] George S. Infrared and Raman characteristic group frequencies: tables and charts. New York: John Wiley & Sons; 2004.